Article

Stabilizing Monoatomic Two-Coordinate Bismuth(I) and Bismuth(II) Using a Redox Noninnocent Bis(germylene) Ligand

Jian Xu, Sudip Pan, Shenglai Yao, Christian Lorent, Christian Teutloff, Zhaoyin Zhang, Jun Fan, Andrew Molino, Konstantin B. Krause, Johannes Schmidt, Robert Bittl, Christian Limberg, Lili Zhao, Gernot Frenking,* and Matthias Driess*

Read Online

ACCESS | Metrics & More | Article Recommendations | SI Supporting Information

ABSTRACT: The formation of isolable monatomic Bi^I complexes and Bi^{II} radical species is challenging due to the pronounced reducing nature of metallic bismuth. Here, we report a convenient strategy to tame Bi^I and Bi^{II} atoms by taking advantage of the redox noninnocent character of a new chelating bis(germylene) ligand. The remarkably stable novel Bi^I cation complex **4**, supported by the new bis(iminophosphonamido-germylene)xanthene ligand $[(P)Ge^{II}(Xant)Ge^{II}(P)]$ **1**, $[(P)Ge^{II}(Xant)Ge^{II}(P) = Ph_2P-(NtBu)_2Ge^{II}(Xant)Ge^{II}(NtBu)_2PPh_2$, Xant = 9,9-dimethyl-xan-thene-4,5-diyl], was synthesized by a two-electron reduction of the cationic $Bi^{III}I_2$ precursor complex **3** with cobaltocene (Cp_2Co) in a molar ratio of 1:2. Notably, owing to the redox noninnocent character of the germylene moieties, the positive charge of Bi^I cation **4** migrates to one of the Ge atoms in the bis(germylene) ligand, giving rise to a germylium(germylene) Bi^I complex as suggested by DFT calculations and X-ray photoelectron spectroscopy (XPS). Likewise, migration of the positive charge of the $Bi^{III}I_2$ cation of **3** results in a bis(germylium)$Bi^{III}I_2$ complex. The delocalization of the positive charge in the ligand engenders a much higher stability of the Bi^I cation **4** in comparison to an isoelectronic two-coordinate Pb^0 analogue (plumbylone; decomposition below $-30\ °C$). Interestingly, **4**$[BAr^F]$ undergoes a reversible single-electron transfer (SET) reaction (oxidation) to afford the isolable Bi^{II} radical complex **5** in **5**$[BAr^F]_2$. According to electron paramagnetic resonance (EPR) spectroscopy, the unpaired electron predominantly resides at the Bi^{II} atom. Extending the redox reactivity of **4**$[OTf]$ employing AgOTf and MeOTf affords $Bi^{III}(OTf)_2$ complex **7** and $Bi^{III}Me$ complex **8**, respectively, demonstrating the high nucleophilic character of Bi^I cation **4**.
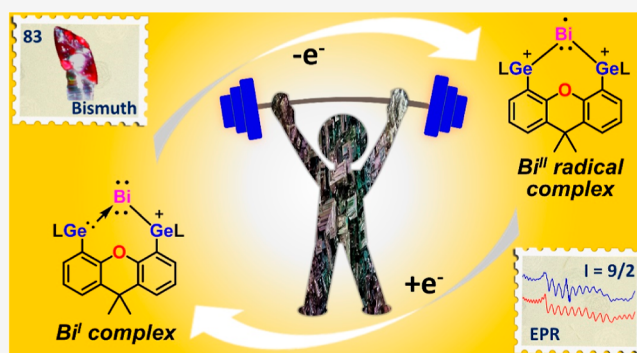
INTRODUCTION

Compounds containing heavy p-block group 14 and 15 elements E in uncommon low oxidation states are of paramount interest because they provide multiple new opportunities for the design of main-group element species mimicking transition-metal-like reactivity with respect to small molecule activation and catalysis.[1−5] However, the synthesis of such isolable species is challenging and requires suitable ligation around the low-valent E atom to prevent E−E bond oligomerization and disproportionation. Recent developments in this direction have paved the way to zerovalent monatomic complexes of the group 14 elements named tetrylones with the general formula L:→E^0←:L (E = C, Si, Ge, Sn, Pb).[6−15] Utilizing the bis(silylene)xanthene,[16] we achieved the whole series of heavier tetrylones previously.[7,11,13,14] The central E^0 atom is two-coordinated by two sufficient donor ligands and obeys the octet rule, retaining its four valence electrons as two lone pairs.[17,18] The various tetrylones stabilized by sufficient Lewis bases show an unparalleled reactivity toward small molecules.[19−22] Monovalent group 15 element complex

cations of the type L_2E^+ (L = donor, E = N, P, As, Sb, Bi)[23−27] are known isoelectronic species but particularly difficult to tame for the heaviest pnictogen, bismuth. Compared with the lighter congeners, low-valent bismuth compounds possess exceptional features such as strong spin−orbit coupling (SOC) due to relativistic effects,[28,29] low redox potentials and transition-metal-like properties in redox catalysis.[30−37] It should be noted here that the peculiar electronic features of low-valent Bi play also a decisive role in rare earth metal−bismuth coordination compounds that are single-molecule magnets.[38−41]

Utilizing the same Lewis donor−acceptor stabilization strategy as previously applied for tetrylones, two examples of
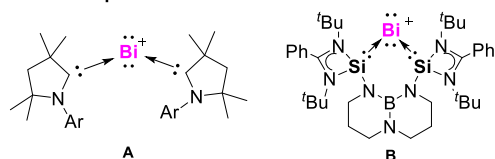
isolable two-coordinate Bi^I cation complexes have been synthesized, namely, cyclic (alkyl)(amino)carbene (cAAC)-supported Bi^I cation complex A^{42} and bis(silylene)-supported Bi^I cation complex B^{23} (Chart 1a). A is only stable in ethereal

Chart 1. (a) Reported Examples of Bi^I Cation Complexes (A,B); (b) Neutral Bi^{II} Radical Complexes (C−E); (c) Cationic Bi^{II} Radical Complexes (F,G); (d) This Work: Bi^I and Bi^{II} Complexes with a Redox Non-innocent Bis(germylene) Ligand^a
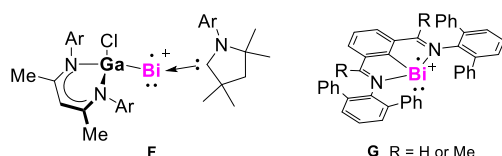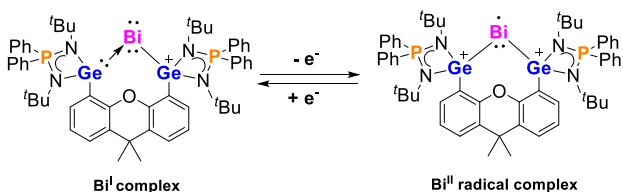

a) Bi^I cation complexes

A   B

b) Neutral Bi^{II} radicals

C   D   E   X = Cl or I

c) Cationic Bi^{II} radicals

F   G   R = H or Me
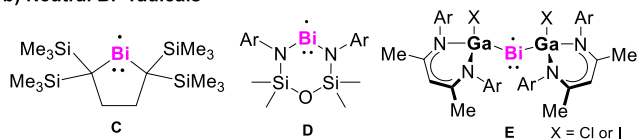
d) This work:

Bi^I complex   − e⁻ / + e⁻ Bi^{II} radical complex

^{a}Ar = 2,6-Diisopropylphenyl.

solutions at relatively high concentrations under an inert atmosphere; dilution of the solution results in its decomposition. The intrinsic lability of Bi^I cation complexes may be attributed to the higher nucleophilicity and electropositive and redox character of the Bi^I site caused by notably larger, diffuse, and polarizable valence orbitals of Bi compared to those of its lighter nonmetallic congeners (N, P, As).[43,44] These electronic features may enable Bi^I cation complexes to act as electron transfer reagents under the concomitant formation of Bi^{II} and Bi^{III} complexes, respectively. However, the redox reactivity of A and B and whether they are suitable precursors for Bi^{II} radical complex are currently unknown. Bi^{II} radical complexes, in turn, are also scarce.[45] Their existence as reactive intermediates[37,46] and transient species[47] has been postulated in previous studies. The unequivocal identification of Bi^{II} radical complexes is challenging, in particular, the electron paramagnetic resonance (EPR) characterization due to the enormous (isotropic and anisotropic) hyperfine interactions and the large nuclear quadrupole moment of the ^{209}Bi nucleus (I = 9/2; 100% natural abundance). Until now, only a few stable monatomic Bi^{II} radicals have been reported (Chart 1b,c).[48−53] Among these, C^{48} is considered a redox radical Bi^{II}/Bi^{III} couple and

lacks observable EPR signals. Compounds D^{49} and $E^{50,51}$ are isolable neutral Bi^{II} radicals with the unpaired electron predominantly residing at the Bi atom. In addition, F^{52} and G^{53} represent known cationic Bi^{II} complexes.

In this work, we present the synthesis and characterization of unprecedented types of remarkably stable monatomic two-coordinate Bi^I and Bi^{II} complexes, which are stabilized by the novel chelating bis(iminophosphonamido-germylene)xanthene ligand $[(P)Ge^{II}(Xant)Ge^{II}(P)]$ **1**, $[(P)Ge^{II}(Xant)Ge^{II}(P)$ = $Ph_2P(NtBu)_2Ge^{II}(Xant)Ge^{II}(NtBu)_2PPh_2$, Xant = 9,9-dimethyl-xanthene-4,5-diyl]. The Bi^I complex **4** can be regarded as an isoelectronic analog of a two-coordinate Pb^0 complex (plumbylone). In contrast to the thermolabile plumbylone analogue, however, which decomposes above −30 °C, **4** is stable even in boiling benzene most likely due to resonance stabilization: the positive charge of the Bi^I cation migrates to one of the germanium atoms in the ligand, giving rise to a (germylium)germylene Bi^I situation as suggested by density functional theory (DFT) calculations. Starting from the Bi^I complex $4[BAr^F]$, the single electron oxidation with ferrocenium BAr^F (Cp_2FeBAr^F, BAr^F = tetrakis[3,5-bis-(trifluoromethyl)phenyl]borate) resulted in the formation of the isolable Bi^{II} radical complex $5[BAr^F]_2$ with the unpaired electron mainly located at the bismuth center, and each germanium atom features one positive charge. Oxidative reactions of $4[OTf]$ with AgOTf and MeOTf (OTf = OSO_2CF_3) afford cationic Bi^{III} complexes, demonstrating the remarkably high nucleophilic character of Bi^I complex **4**.

■ RESULTS AND DISCUSSION

Synthesis and Characterization of Monoatomic Bi^I Complexes 4[BAr^F] and 4[OTf]. At first, we prepared the starting material for **1**, the N-heterocyclic iminophosphonami-do-chlorogermylene, **(P)GeCl** $[Ph_2P(NtBu)_2GeCl]$, through salt metathesis reaction of iminophosphonamide with NEt_3 and $GeCl_2$·dioxane in THF at −78 °C (see the Supporting Information). The latter is characterized by NMR spectroscopy, electrospray ionization (ESI) mass spectrometry, and X-ray diffraction (XRD) analysis (see the Supporting Information). Compared to N-heterocyclic amidinato-chlorogermylene $[PhC(NtBu)_2GeCl]$,[54] the phosphorus atom in **(P)GeCl** increases the σ-donor ability of germylene due to the $N^−−P^+$ bond polarity.[55] The latter is well supported by DFT calculations of **(P)GeCl** and related amidinato-chlorogermylene (see the Supporting Information, Figure S66).

Starting from **(P)GeCl**, chelating ligand **1** is readily accessible in a one-pot synthesis (Scheme 1). Dilithiation of 4,5-dibromo-9,9-dimethylxanthene with 2 M equiv of s-BuLi in Et_2O, followed by a salt metathesis reaction with **(P)GeCl**, afforded the desired bis(iminophosphonamido-germylene)-xanthene **1** as a yellow powder in 72% yield. Its $^{31}P\{^1H\}$ NMR spectrum shows a singlet at δ 26.6 ppm. The molecular structure of **1** established by XRD analysis reveals a Ge···Ge distance of 4.071 Å, excluding attractive interaction between the two Ge atoms (Figure 1). Compared to bis(amidinato germylene)xanthene,[56] compound **1** is a stronger chelating bis(germylene) ligand due to the P−N bond polarization mentioned above.

Treatment of **1** with 1 M equiv of BiI_3 in THF at room temperature led to the formation of **2** as a brown powder in 85% yield. The iodide counteranion in **2** can be easily displaced by BAr^F and OTf anion upon mixing of **2** with 1 M equiv of $NaBAr^F$ or AgOTf in dichloromethane (DCM),

Scheme 1. Synthesis of Bis(germylene) 1 and Bi^III I_2 Precursors 2 and 3
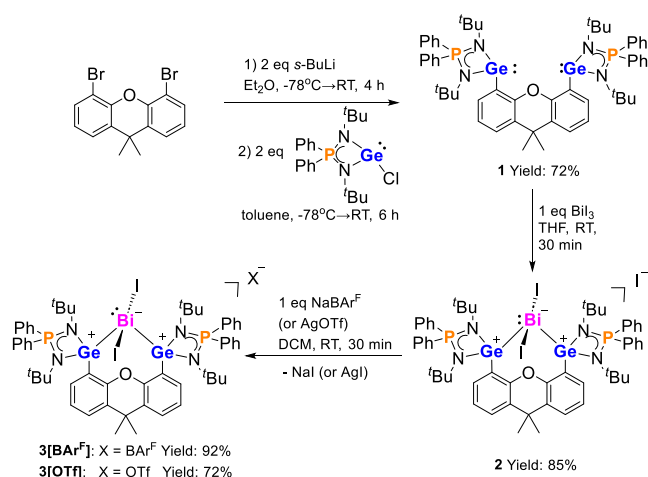
affording **3[BAr^F]** (yield: 92%) and **3[OTf]** (yield: 72%) as orange powders, respectively (Scheme 1). As expected, the ^1H NMR spectra of **2**, **3[BAr^F]**, and **3[OTf]** are practically identical. The $^{11}B\{^1H\}$ NMR spectrum of **3[BAr^F]** shows a singlet at δ −6.6 pm, which is attributed to the BAr^F anion. The $^{19}F\{^1H\}$ NMR signal of **3[OTf]** (δ −78.8 ppm) indicates the presence of a "free" OTf anion.[24] The $^{31}P\{^1H\}$ NMR spectra of **2**, **3[BAr^F]**, and **3[OTf]** exhibit a singlet at δ 54.6 ppm, which is significantly downfield shifted compared to that of **1** (δ 26.6 ppm). The molecular structures of **2**, **3[BAr^F]**, and **3[OTf]** were determined by XRD analysis (Figure 1; also see the Supporting Information). In each of these compounds, a stereoactive lone pair is present on the four-coordinate bismuth atom with a central Bi^III atom adopting a seesaw geometry with two iodine atoms located in axial positions (I1−Bi1−I2:169.779(15)-174.507(10)°). The Ge1−Bi1−Ge2 angles range from 103.895(14) to 109.244(18)°. It is worth noting that **2**, **3[BAr^F]**, and **3[OTf]** are the first examples of germylene Bi^III halide complexes.

With the cationic Bi^III I_2 precursors **2**, **3[BAr^F]**, and **3[OTf]** in hand, we envisioned that the monatomic Bi^I complex could be obtained through their reductive deiodination. The reaction of **2** with 2 M equivs of KC_8 or {(ArNacnac)Mg^I}_2[57] in THF led to decomposition of **2** most likely due to overreduction. To our delight, the reactions of **3[BAr^F]** and **3[OTf]** with 2 M equivs of cobaltocene (Cp_2Co) in toluene (**3[BAr^F]**) and THF (**3[OTf]**) at room temperature gave red solutions, from which **4[BAr^F]** and **4[OTf]** were isolated as red crystals in 83 and 45% yields, respectively (Scheme 2). Featuring the same cation moiety, the ^1H NMR spectra of both products reveal a singlet at the same chemical shift (δ 1.08 ppm) for the *tert*-butyl groups, implying that cation **4** is symmetric and solvent is separated in solution. Accordingly, the $^{31}P\{^1H\}$ NMR spectra of **4[BAr^F]** and **4[OTf]** exhibit a singlet at the same chemical shift of δ 44.5 ppm, significantly upfield shifted compared to those of **2** and **3** (δ 54.6 ppm), but downfield shifted compared to that of **1** (δ 26.6 ppm), respectively. The $^{11}B\{^1H\}$ NMR spectrum of **4[BAr^F]** shows a sharp singlet at δ −6.6 ppm, corresponding to the weakly coordinating BAr^F anion, and the $^{19}F\{^1H\}$ NMR spectrum of **4[OTf]** shows a signal at −78.9 ppm for the "free" OTf anion.[24] Notably, a two-electron oxidation of **4** with I_2 in DCM-d_2 after 5 min at room temperature restored compound **3** in quantitative yield.
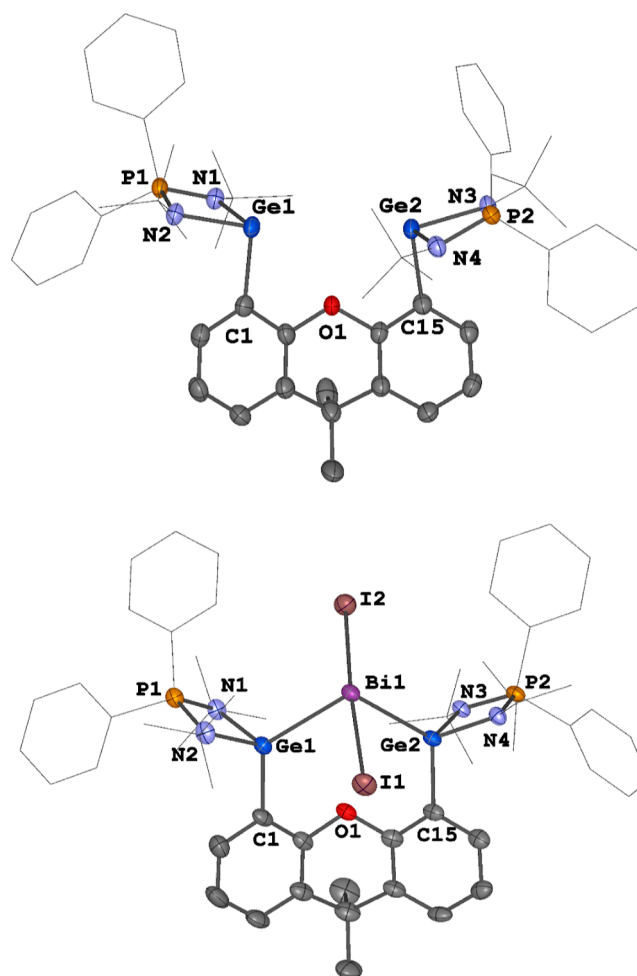

Figure 1. Molecular structures of **1** (top) and the cations in **2**, **3[BAr^F]** and **3[OTf]** (bottom). Thermal ellipsoids are drawn at the 50% probability level. H atoms, anionic moieties and solvent molecules are omitted for clarity. Selected bond lengths (Å) and angles (deg): **1**: Ge1−C1 2.0607(15), Ge2−C15 2.0458(15), N1−Ge1−C1 99.11(5), N2−Ge1−C1 96.42(5), N3−Ge2−C15 99.21(5), N4−Ge2−C15 92.06(5). **2**: Bi1−Ge1 2.7578(6), Bi1−Ge2 2.7497(6), Bi1−I1 3.0921(5), Bi1−I2 2.9991(4), I1−Bi1−I2 169.779(15), Ge1−Bi1−Ge2 109.244(18). **3[BAr^F]**: Bi1−Ge1 2.7737(5), Bi1−Ge2 2.7800(5), Bi1−I1 3.0406(3), Bi1−I2 3.0424(3), I1−Bi1−I2 172.326(10) Ge1−Bi1−Ge2 103.895(14). **3[OTf]**: Bi1−Ge1 2.8035(5), Bi1−Ge2 2.7813(5), Bi1−I1 3.0404(3), Bi1−I2 3.0679(3), I1−Bi1−I2 174.507(10), Ge1−Bi1−Ge2 106.995(16).

Scheme 2. Synthesis of 4 and Reversible Interconversion of 3 and 4 with I_2
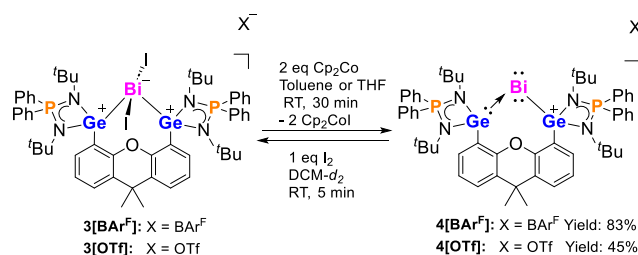
4[BAr^F] crystallized in the triclinic space group $P\bar{1}$, while **4[OTf]** crystallized in the orthorhombic space group *Pbca*. Both structures were elucidated by XRD analysis and exhibit

separated ion-pair structures with an almost identical Bi^I complex (Figure 2). The central Bi^I site is bonded to the
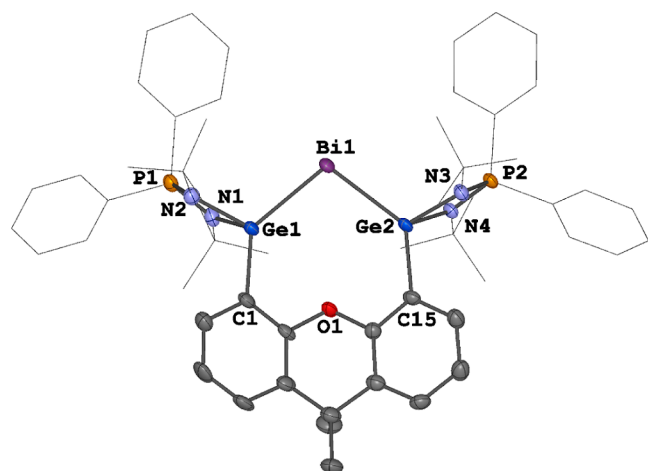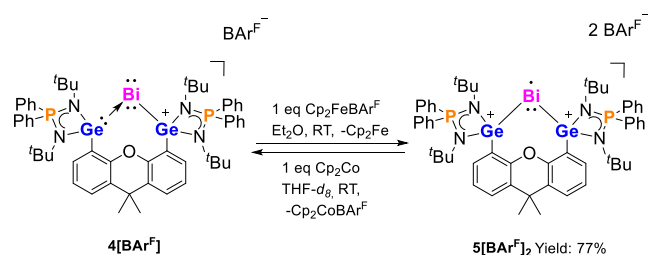

Figure 2. Molecular structures of the cation **4** in **4**[BAr^F] and **4**[OTf]. Thermal ellipsoids are set at the 50% probability. Hydrogen atoms, counteranions and solvent molecules are omitted for clarity. Selected distances (Å) and angles (deg): **4**[BAr^F]: Bi1–Ge1 2.6672(4), Bi1–Ge2 2.6627(4), Ge1–Bi1–Ge2 103.981(12). **4**[OTf]: Bi1–Ge1 2.6693(9), Bi1–Ge2 2.6712(9), Ge1–Bi1–Ge2 104.67(3).

two Ge atoms with Ge–Bi distances ranging from 2.6627(4) to 2.6712(9) Å, the latter are significantly shorter than those observed in **3** [2.7737(5)–2.8035(5) Å], which is consistent with the decrease of the coordination number of the Bi atom in **4** compared to its precursor **3**. The Ge1–Bi1–Ge2 angles of 103.981(12)° (**4**[BAr^F]) and 104.67(3)° (**4**[OTf]) are quite similar to those of **3**[BAr^F] (103.895(14)°) but slightly smaller than those of **2** (109.244(18)°) and **3**[OTf] (106.995(10)°), respectively. However, the Ge1–Bi1–Ge2 angles are significantly larger than the Si1–Bi1–Si2 angle of the Bi^I cation complex **B** (82.10(3)°) due to the larger ring size.[23]

Single-Electron Transfer Reactions. Owing to the presence of two lone pairs of electrons on the Bi^I center in **4**, we envisaged that **4** is a suitable precursor for the synthesis of Bi^{II} and Bi^0 radical complexes via single-electron oxidation/reduction reactions. This is supported by the cyclic voltammetry (CV) analysis of compound **4**[BAr^F]. The CV exhibits two quasi-reversible oxidation processes at $E_{1/2} \approx$ −0.54 V and −0.09 V, followed by a third irreversible oxidation wave at $E_{p,a}$ = 0.66 V vs Fc/Fc$^+$ and an irreversible reduction wave at $E_{p,c}$ = −1.53 V vs Fc/Fc$^+$ (see the Supporting Information, Figure S29). To examine this hypothesis, we carried out single-electron oxidation reactions of **4**[BAr^F]. The latter was reacted with 1 M equiv of Cp$_2$Fe[BAr^F] in Et$_2$O, furnishing the desired Bi^{II} radical complex **5**[BAr^F]$_2$ in 77% yield (Scheme 3). Complex **5**[BAr^F]$_2$ is a brownish powder in the solid state and highly air-sensitive, but it can be stored under a N$_2$ atmosphere at −30 °C for several weeks. In addition, treatment of **5**[BAr^F]$_2$ with 1 M equiv of Cp$_2$Co in THF for 5 min at room temperature restored compound **4**[BAr^F] in quantitative yields. We also conducted the single-electron reduction of **4**[BAr^F] in an attempt to synthesize neutral Bi^0 compound **6**. When one molar equiv of Cp$_2$Co or KC$_8$ was reacted with **4**[BAr^F] in THF at −78 °C, the reaction ultimately resulted at ambient temperature in formation of elemental bismuth as a precipitate due to decomposition.

Scheme 3. Reversible Interconversion of 4[BAr^F] and 5[BAr^F]$_2$

XRD analysis revealed that compound **5**[BAr^F]$_2$ is an ion triple that crystallizes in the triclinic space group $P\bar{1}$ and contains the monatomic Bi^{II} moiety **5** as shown in Figure 3.
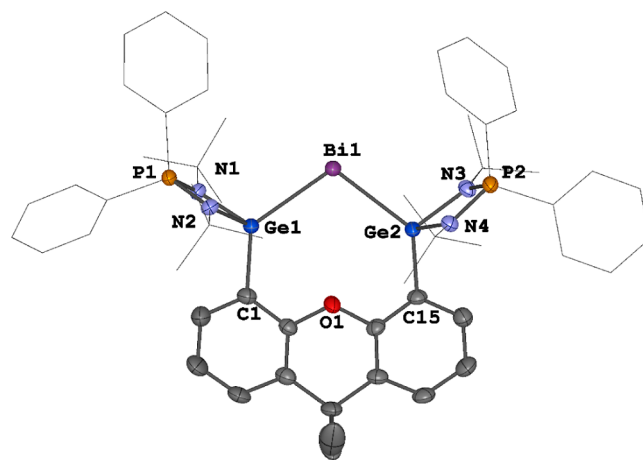

Figure 3. Molecular structure of the radical dication **5** in **5**[BAr^F]$_2$. Thermal ellipsoids are set at the 50% probability. Hydrogen atoms, anionic moieties and solvent molecules are omitted for clarity. Selected bond lengths (Å) and angles (deg): Bi1–Ge1 2.7112(3), Bi1–Ge2 2.7147(3), Ge1–Bi1–Ge2 107.583(9).

Similar to **4**[BAr^F], **5**[BAr^F]$_2$ features a two-coordinate Bi^{II} center, but there are two separated BAr^F counteranions present in the molecular structure, indicating that **5**[BAr^F]$_2$ is a Bi^{II} radical complex. The Ge1–Bi1–Ge2 angle of 107.583(9)° in **5**[BAr^F]$_2$ is slightly larger than that of **4** in **4**[BAr^F] (103.981(12)°) and **4**[OTf] (104.67(3)°). Additionally, the Ge–Bi distances (2.7112(3) and 2.7147(3) Å) of **5**[BAr^F]$_2$ are slightly longer than those of **4** (2.6627(4)–2.6712(9) Å) but shorter than those of **3** (2.7737(5)–2.8035(5) Å), presumably due to the weaker π-back-donation from the Bi^{II} center to both Ge atoms in **5**[BAr^F]$_2$.

Compound **5**[BAr^F]$_2$ is paramagnetic and shows broad resonance peaks in the solution ^{1}H NMR spectrum at room temperature (see the Supporting Information, Figure S37). The effective magnetic moment (μ_{eff}) of a microcrystalline solid sample, measured with a superconducting quantum interference device (SQUID) magnetometer, is temperature-dependent (see the Supporting Information, Figure S60). The magnetic moment linearly decreases with decreasing temperature and shows a value of 1.98 μ_B at 300 K, which is comparable to reported Bi^{II} radical compounds.[49,50,53] The latter value is consistent with a single unpaired electron $S = 1/2$ system.

EPR spectroscopy was applied to explore the electronic nature of the Bi^{II} radical complex **5**[BAr^F]$_2$ in more detail. The

continuous-wave X-band (9 GHz) and pseudomodulated Q-band field swept echo (34 GHz) spectra, respectively (see the Supporting Information, Figure S61), exhibit a very broad multiline EPR signal with components spanning the whole experimentally accessible spectral range. As a consequence of the typically very strong hyperfine coupling of ^{209}Bi (I = 9/2) in the GHz range, yet moderate g-anisotropy, the number of EPR transitions monitored at X-band and Q-band frequencies are limited and much higher magnetic field is required to decouple g-matrix and A-tensor and completely resolve the EPR spectrum. Thus, we used W-band (94 GHz) EPR and obtained a quite well-resolved multiplet of lines with recognizable g-anisotropy, yielding for each g-component 10 lines, which partially overlap with each other (Figure 4). The
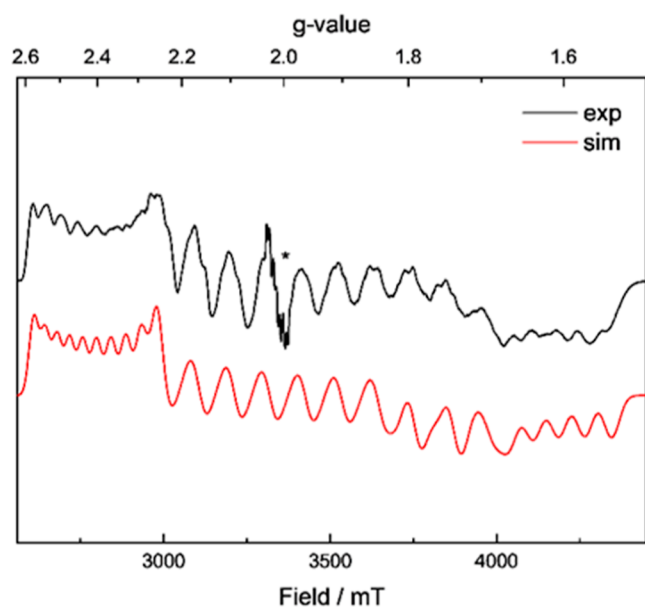

Figure 4. Pseudomodulated W-band field swept echo EPR-spectrum of **5**[BAr^F]$_2$ recorded at 10 K. The experimental spectrum is displayed as black and the corresponding simulation as red line. The g-matrix derived from the simulation is g = [2.39, 1.92, 1.66] and the hyperfine coupling A = [1370, 2920, 1650] MHz. The signal labeled by an asterisk is related to an impurity from manganese.

simulation of the experimental data resulted in the following g-matrix principal values of g = [2.39, 1.92, 1.66] for an S = 1/2 system and the hyperfine tensor principal values A = [1370, 2920, 1650] MHz, with the largest A-component along the intermediate g-component. The average g value ($g_{av} = (g_1 + g_2 + g_3)/3$) of **5**[BAr^F]$_2$ is g_{av} = 1.99 and rather close to the free electron g, as observed for the gallium-stabilized Bi radicals **E** and **F**[58], but distinctly different from the nitrogen-coordinated Bi radicals **D**[49] and **G**[53], which show a g_{av} significantly smaller than 2. All EPR values of **G** refer only to the protonated compound (R = H); the methylated variant (R = Me) has almost identical values. The symmetry of the hyperfine tensor of **5**[BAr^F]$_2$ corresponds to that of **E** and **F**,[58] which is also aligned with its largest component along the intermediate g-component. In contrast, the hyperfine tensors reported for **D**[49] and **G**[53] are aligned with their largest component along the smallest g-component. The magnitude of the hyperfine coupling of **5**[BAr^F]$_2$ with an average value ($A_{av} = (A_1 + A_2 + A_3)/3$) A_{av} = 1980 MHz is intermediate between the smaller A_{av} = 1383 MHz and A_{av} = 1650 MHz of **E** and **F**,[58]

respectively, and the larger A_{av} = 3799 MHz and A_{av} = 3180 MHz reported for **D**[49] and **G**[53], respectively. The axial part T of the hyperfine coupling ($T = ((A_1 + A_3)/2 - A_{iso})$) found here for **5**[BAr^F]$_2$ with T = −470 MHz is in its absolute value again clearly larger than that found for **E** and **F** (−245 MHz and −333 MHz)[58] and very similar to the axial parts given for **D**[49] and **G**[53] with T = −498 MHz and T = −462 MHz, respectively. Following the parameters, A_{av} and T can be used to estimate the spin density in the Bi 6s and 6p orbitals according to Morton and Preston.[59] The A_{av} = 1980 MHz of **5**[BAr^F]$_2$ yields with the A = 77,530 MHz[59] for a 100% occupied Bi 6s (obtained assuming g = 2.0023) a population P_{6s}(Bi) ≅ 0.03. The T = −470 MHz of **5**[BAr^F]$_2$ on the other hand yields with the P = 1659 MHz[59] for a 100% occupied Bi 6p orbital and the angular factor −2/5 a population P_{6p}(Bi) ≅ 0.71. Thus, the SOMO orbital of **5**[BAr^F]$_2$ has predominant 6p character with only a small admixture of 6s in agreement with the DFT results (see below) and the findings for the other Bi radicals **D**, **E**, **F** and **G**.[49−53,58] A total Bi spin population of about 3/4 is deduced from the EPR spectrum, suggesting substantial spin delocalization into the ligand as reported also for **E** and **F**.[58] Significantly less spin delocalization is reported for **D**[49] and **G**[53]. This might at first sight contradict the small difference between the T-values of **5**[BAr^F]$_2$ and **G**[53] with −470 and −462 MHz, but can immediately be explained by the significantly different g_{av}-values (1.99 and 1.79, respectively) of the two radicals. The larger g_{av} of **5**[BAr^F]$_2$ induces a larger magnetic moment, which partially compensates for the higher Bi spin density in **G** for the resulting hyperfine couplings. This effect explains the significantly different P_{6p}(Bi) values deduced for **5**[BAr^F]$_2$ and **G** at rather similar T values. The interpretation of the different total P(Bi) spin densities for the complexes in terms of spin delocalization into the ligands has to be taken with care since the analysis following Morton and Preston[59] is based on the assumption of atomic Bi 6s and 6p orbitals and can only give estimates. Quantitative comparison with DFT data requires information about ligand hyperfine couplings. Unfortunately, the direct neighbor Ge of Bi in **5**[BAr^F]$_2$ has only a relatively low abundance with ^{73}Ge (7.76%) and a high spin stable isotope with I = 9/2, which is a rather bad reporter for spin delocalization into the ligand, and produces no discernible splitting in the EPR spectrum, making hyperfine selective methods necessary for obtaining further information.

DFT Calculations. DFT calculations at the BP86-D3(BJ)/def2-TZVP level were performed to shed light on the electronic structure, stability, and chemical bonding of monocation **4**, and radical dication **5**. For completeness, we also calculated the hypothetical neutral analogue Bi^0 compound **6**. Figure S71 shows the calculated geometries of the three compounds and the most important bond lengths and angles. It is interesting to note that the calculated Bi−Ge distances in neutral **6** (2.654 Å) stay nearly the same in cation **4** (2.655 Å) but are slightly longer in radical dication **5** (2.715 Å). The cation **4** has an electronic singlet ground state with a triplet state of 29.6 kcal mol^{-1} higher in energy, while **5** and **6** have doublet ground states where the quartet states are higher in energy by 47.7 and 29.3 kcal mol^{-1}, respectively. The theoretical values for **4** and **5** are in very good agreement with the experimental data.

The energy minimum structure of neutral **6** has C_s symmetry. The geometry optimizations of **4** and **5** gave structures which are slightly distorted from C_s symmetry.

	4		**5**

LP on Bi: s(90%) p(10%) ON: 1.94

Bi1-Ge2 π bond: (90%)Bi1: p(100%); (10%)Ge2: s(1%) p(99%); ON: 1.76

LP on Bi: s(90%) p (10%); ON: 1.96

LP on Bi: p(100%): ON: 0.91

Bi1-Ge2 σ bond: (40%)Bi1: s(5%) p(95%); (60%)Ge2: s(47%) p(53%); ON: 1.93

Bi1-Ge2′ σ bond: (40%)Bi1: s(5%) p(95%); (60%)Ge2′: s(47%) p(53%); ON: 1.93

Bi1-Ge2 σ bond; (45%)Bi1: s(5%) p(95%) (55%)Ge2: s(32%) p(68%); ON: 1.92

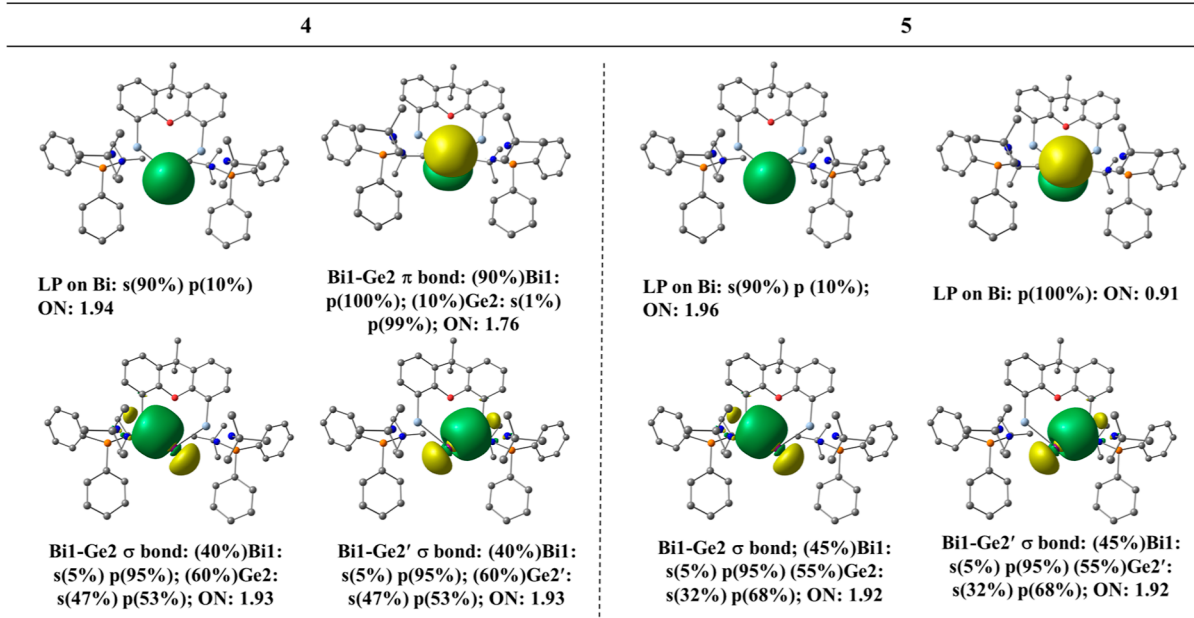Bi1-Ge2′ σ bond: (45%)Bi1: s(5%) p(95%) (55%)Ge2′: s(32%) p(68%); ON: 1.92

Figure 5. Natural orbitals and their AO compositions of cation **4** (left) and the radical dication **5** (right).

Calculations with enforced C_s symmetry gave structures which have very small imaginary frequencies (2.4i for **4** and 9.4i for **5**) even after using a superfine grid. The energy difference between the C_s structures and the energy minima are >0.1 kcal mol^{-1} for **4** and 0.4 kcal mol^{-1} for **5** and the differences in the bond lengths and angles are negligible. We decided to use the C_s structures shown in Figure S71 (see the Supporting Information) for the bonding analysis for simplicity, which does not affect our conclusion.

The energetically most favorable reaction pathways for rupture of the Ge−Bi bonds in **4**, **5** and **6** suggest that bismuth dissociates always as neutral Bi atom even from radical dication **5**. This is in line with the calculated charge distribution. The NBO atomic charges on Bi are −0.23e in **4** and 0.26e in **5**. Notably, the partial charge on Bi in neutral **6** (−0.25e) is nearly the same as that in cation **4**. The calculated values of the bond dissociation energy (BDE) are D_e = 62.2 kcal mol^{-1} for neutral **6**, D_e = 87 kcal mol^{-1} for cation **4** and D_e = 64.1 kcal mol^{-1} for the radical dication **5**. The zero-point energy (ZPE) and thermal corrections (see Supporting Information, Figure S71) suggest that all three compounds are thermodynamically stable with respect to liberation of Bi^0. It is amazing that the BDE for the dissociation of neutral **6** and radical dication **5** has nearly the same value. The difficulty in isolating neutral **6** can be explained by its very low ionization potential (IP). Notably, the calculated adiabatic IP for **6** is only 3.55 eV at the BP86-D3(BJ)/def2-TZVP level, which is even much less than for the cesium atom (4.04 eV at the BP86-D3(BJ)/def2-TZVP), 3.89 eV experimentally.[60]

We analyzed the bonding situation in **4** and **5** in more detail using a variety of methods. Figure 5 shows the natural orbitals that are related to the valence state of Bi in the two compounds. In **4**, there is a σ lone pair orbital at Bi with 90% s character and a strongly polarized Bi−Ge π orbital, which is 90% localized at Bi that mimics a π lone-pair orbital. There are two Bi−Ge σ-bonding orbitals which are slightly polarized toward Ge. The Bi atom in **4** has two lone-pair orbitals. The HOMO and HOMO − 2 of **4** correspond to a π-type and a σ-type lone pair at the Bi^I center, respectively, which is a

characteristic feature of ylidones L→E←L, the heavy-atom homologues of carbones L→C←L (Figure 6a).[18,61−64] The

a)

HOMO
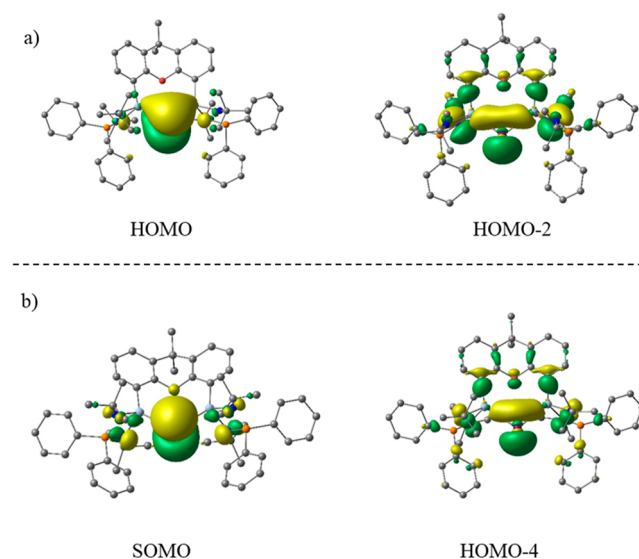
HOMO-2

b)

SOMO

HOMO-4

Figure 6. Molecular orbitals of cation **4** (a) and radical dication **5** (b).

orbitals of the radical dication **5** are very similar but the π lone-pair orbital is occupied by only one electron, which may better be named as "lone single orbital" (Figure 6b). The NBO spin density of 0.87e on Bi also supports this assignment (see the Supporting Information, Figure S74 for the spin density plot). The unpaired electron in a π-type orbital is in agreement with the EPR data, showing a small s character and a predominant p orbital character of the unpaired electron.

The NBO orbitals of **4** and **5** support the Lewis structures shown in Scheme 4. A more detailed analysis using the EDA-NOCV method reveals a bonding situation that is more complex than that described by the Lewis structure. We carried out EDA-NOCV calculations of **4** and **5** using Bi and the bis(germylene) ligand L with different charges and different

Scheme 4. Main Resonance Structures of Cation 4 and Radical Dication 5, Respectively[a]
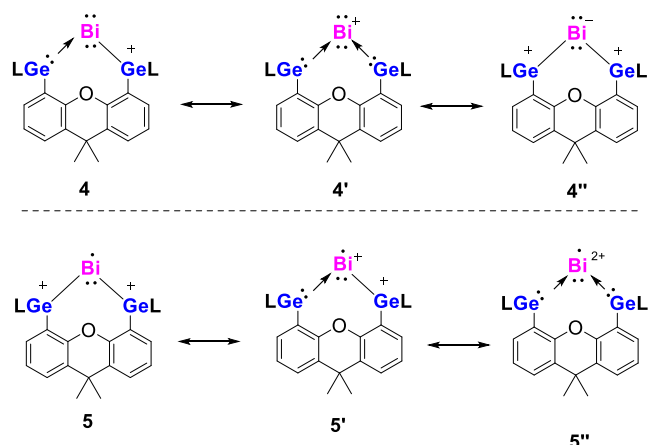
[a]L = Ph$_2$P(NtBu)$_2$.

electron configurations (see the Supporting Information, Tables S25 and S26). Table 1 shows the numerical results with the fragments that give the smallest energy values for the orbital interaction ΔE_{orb}, indicating the most favorable moieties for describing the bonding situation.[65−70] It turned out that the best description of the L(Ge)-Bi bonds in 4 and 5 has neutral Bi and singly or doubly charged ligand in the given electron configurations, which agrees with the calculated partial charges given by the NBO method. The electronic reference states of Bi are the ^{2}D excited state for 4 and the ^{4}S ground state for 5 whereas the ligands L$^+$ and L^{2+} have doublet and triplet states, respectively.

The breakdown of the total orbital interactions ΔE_{orb} in pairwise contributions shows that in 4 and 5 there are two large σ terms $\Delta E_{orb(1)}$ and $\Delta E_{orb(2)}$ and one weaker π term $\Delta E_{orb(3)}$, which can be identified by inspecting the associated deformation densities displayed in Figure 7. The radical dication 5 has two electron-sharing σ Ge−Bi−Ge interactions and one very weak π Ge←Bi→Ge back-donation of the singly occupied π orbital at Bi. This supports the bonding, as suggested by the NBO method and depicted by the Lewis structure shown in Scheme 4. The EDA-NOCV results for cation 4 suggest that the two Ge−Bi−Ge σ bonds actually arise from one dative interaction into the vacant 6p$_{\pi\parallel}$ AO of Bi Ge→Bi(6p$_{\pi\parallel}$)←Ge (+,−) but the second σ bond comes from

$\Delta E_{orb(1)}$ = -81.0; |$\nu_{1\alpha/1\beta}$| = 0.62/0.63 $\Delta E_{orb(1)}$ = -69.2; |$\nu_{1\alpha/1\beta}$| = 0.59/0.61

$\Delta E_{orb(2)}$ = -61.3; |ν_2| = 0.84 $\Delta E_{orb(2)}$ = -77.1; |$\nu_{2\alpha/2\beta}$| = 0.49/0.66

$\Delta E_{orb(3)}$ = -17.6; |ν_3| = 0.49 $\Delta E_{orb(3)}$ = -6.0; |$\nu_{3\alpha}$| = 0.18
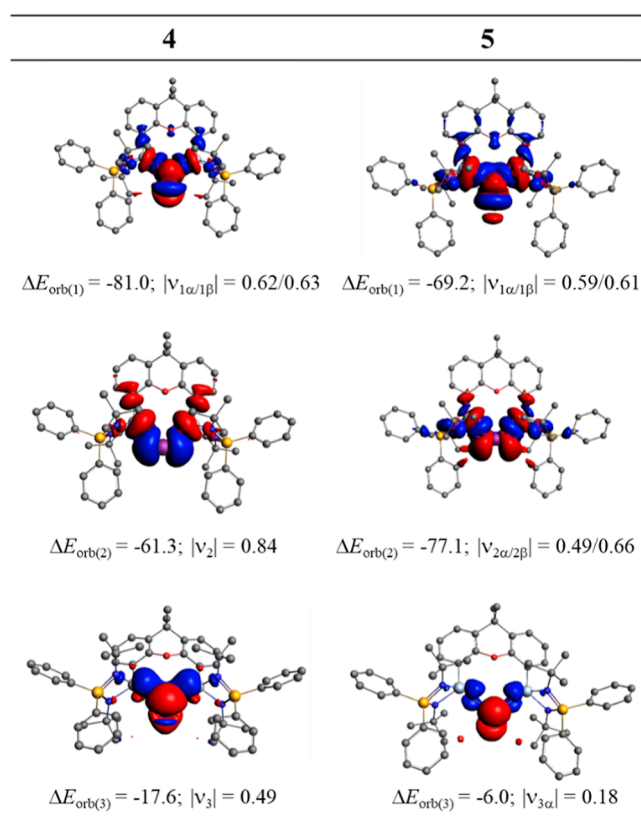
Figure 7. Plot of the deformation densities $\Delta\rho_{(1)}−\Delta\rho_{(3)}$ which are associated with the pairwise orbital interactions $\Delta E_{orb(1)}−\Delta E_{orb(3)}$ of cation 4 and radical dication 5. The eigenvalues ν are a measure for the relative amount of charge transfer. The direction of the charge flow is red → blue.

electron-sharing interactions of the singly occupied 6p$_\sigma$ AO of bismuth, Ge−Bi(6p$_\sigma$)−Ge. Such a detail of the interatomic interactions cannot adequately be sketched by a Lewis structure. It does not invalidate the description given by the Lewis structure shown in Scheme 4 but underlines the fact that the actual interatomic interactions are more complex than those suggested by Lewis formulas. We thus propose the relevance of the main resonance structures 4′, 4″, 5′ and 5″ (Scheme 4). The increase in the oxidation states of the Ge atoms in 4 and 5 is in line with the Ge(3d) binding energies obtained by X-ray photoelectron spectroscopy (XPS) (see

Table 1. Results of EDA-NOCV Calculations of Cation 4 and Radical Dication 5 at the BP86-D3(BJ)/TZ2P-ZORA//BP86-D3(BJ)/def2-TZVP Level Using the Most Favorable Fragment Partitioning Schemes[a]

energy	orbital interaction	4 Bi (^{2}D, 6s^{2}6p$_{\pi\perp}$^{2}6p$_\sigma$^{1}6p$_{\pi\parallel}$^{0}) + L$^+$ (doublet)	5 Bi (^{4}S, 6s^{2}6p$_{\pi\perp}$1$6p_\sigma$^{1}6p$_{\pi\parallel}$^{1}) + L^{2+} (triplet)
ΔE_{int}		−147.0	−124.6
ΔE_{Pauli}		204.2	240.3
ΔE_{disp}[b]		−26.2 (7.5%)	−27.3 (7.5%)
ΔE_{elstat}[b]		−154.8 (44.1%)	−171.7 (47.1%)
ΔE_{orb}[b]		−170.2 (48.5%)	−165.9 (45.5%)
$\Delta E_{orb(1)}$[c]	Ge−Bi(6pσ)−Ge electron-sharing (+,+) σ bond	−81.0 (47.6%)	−69.2 (41.7%)
$\Delta E_{orb(2)}$[c]	Ge→Bi(6p$_{\pi\parallel}$)←Ge (+,−) σ donation	−61.3 (36.0%)	
$\Delta E_{orb(2)}$[c]	Ge−Bi(6p$_{\pi\parallel}$)−Ge electron-sharing (+,−) σ bond		−77.1 (46.5%)
$\Delta E_{orb(3)}$[c]	Ge←Bi(6p$_{\pi\perp}$)→Ge π-backdonation	−17.6 (10.3%)	−6.0 (3.6%)
$\Delta E_{orb(rest)}$[c]		−10.3 (6.1%)	−13.6 (8.2%)

[a]Energy values are given in kcal mol^{-1}. [b]The percentage contribution with respect to total attraction is given in parentheses. [c]The percentage contribution in parentheses is given with respect to total orbital interaction.

Supporting Information, Figure S64). In fact, the values of **4** (32.38 eV) and **5** (32.48 eV) are significantly blue-shifted in comparison with that of the Ge^{II} atoms in the "free" bis-germylene **1** (30.88 eV).

Detailed inspection of the deformation densities reveals further interesting electronic information. The charge flow red → blue associated with $\Delta E_{orb(1)}$ shows an area charge accumulation at Bi for both compounds **4** and **5** that stems from the hybridization of the 6s/6p$_\sigma$ AOs.

We also analyzed the electronic charge in **4** and **5** with the quantum theory of atoms in molecules (QTAIM) method developed by Bader.[71] Figure 8 shows the Laplacian
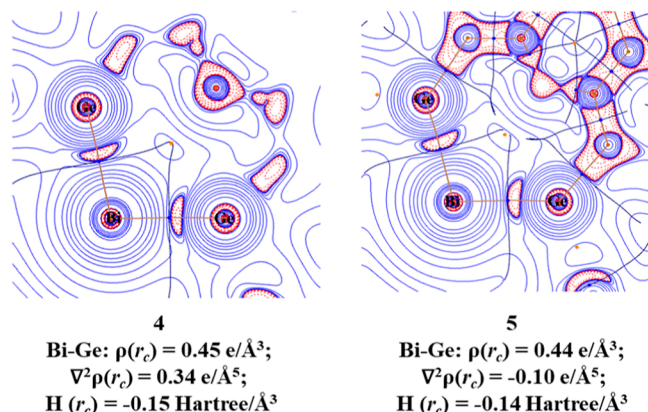

Figure 8. Contour plot of the Laplacian of electron density of cation **4** and radical dication **5** in the Ge−Bi−Ge plane calculated at the BP86-D3(BJ)/def2-TZVP level. Red lines indicate areas of charge concentration [$\nabla^2\rho(r) < 0$] and blue lines show areas of charge depletion [$\nabla^2\rho(r) > 0$].

distribution of electron density $\nabla^2\rho(r)$ in the Ge−Bi−Ge planes of the two compounds. As expected, there are bond critical points (BCPs) for the Bi−Ge bonds where the areas of charge accumulation ($\nabla^2\rho(r) < 0$, indicated by red dotted lines) are closer to the Ge atoms, signaling a polarization of the bonds toward Ge. The negative values of the energy density $H(r_c)$ at the BCPs are characteristic of covalent interactions.[72] Note that there is no area of charge accumulation for the σ lone-pair electrons at Bi, because the 6s AO of the latter is very diffuse.

We carried out further calculations on the precursor **3** precursor. The computed distances and angles are in good agreement with the experimental data (Supporting Information, Figure S67). Remarkably, the NBO analysis revealed that the BiI$_2$ moiety carries an overall negative charge of $-0.45e$ (Bi: 0.46e; I1: $-0.48e$; I2: $-0.43e$) and the ligand has a positive charge of +0.55e. EDA-NOCV calculations using the fragments BiI$_2$ and the ligand L with charges and electronic state showed that the best description is given by BiI$_2^-$ (ate-type) and L^{2+} (T) in the electronic triple state, which give two electron-sharing Bi-L single bonds (see the Supporting Information, Table S24, Figure S68). This agrees with the shape of the natural orbitals of **3** suggested by the NBO analysis (see the Supporting Information, Figure S69). A lone-pair orbital at Bi is found in the NBO analysis, and it also appears as dominant part of the HOMO of **3** (see the Supporting Information, Figure S70). The EDA-NOCV and NBO methods suggest that the best description of the bonding situation of **3** is sketched as in Scheme 2.

Reactivity of Bi^I Complex 4[OTf] toward AgOTf.

Interestingly, the CV of **4**[OTf] exhibits two quasi-reversible oxidation processes at $E_{1/2} \approx -0.46$ V and -0.1 V and an irreversible oxidation wave at $E_{p,a} = 0.44$ V vs Fc/Fc$^+$ (see the Supporting Information, Figure S36). Upon adding 1 M equiv of AgOTf to **4**[OTf] in DCM, only half of **4**[OTf] was consumed. NMR monitoring showed that a new compound was formed in the solution along with a black metallic precipitate. We thus speculated that a two-electron oxidation reaction occurred and compound **7** was furnished (Scheme 5).

Scheme 5. Reaction of 4[OTf] with AgOTf
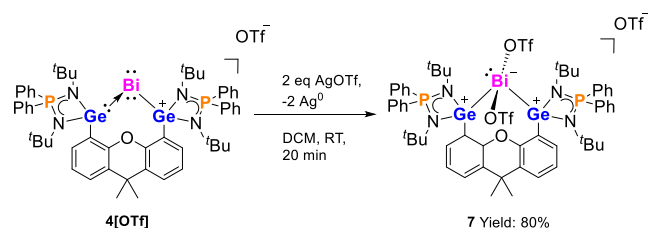
When two molar equivalents of AgOTf were added, nearly all of **4**[OTf] was converted to **7**. After workup, **7** was isolated as a yellow powder in 80% yield. The ^{31}P{^{1}H} NMR spectrum of **7** displays a singlet at $\delta = 58.9$ ppm. The ^{19}F{^{1}H} NMR spectrum shows two signals at $\delta = -76.9$ and $\delta = -78.6$ ppm, indicating that the OTf anions have two distinct chemical environments. Notably, a lighter congener Sb^I cation undergoing Sb^I→Ag^I coordination with AgOTf, instead of the two-electron oxidation, was recently reported.[26]

The molecular structure of compound **7** was confirmed by XRD analysis (Figure 9). Compound **7** crystallizes in
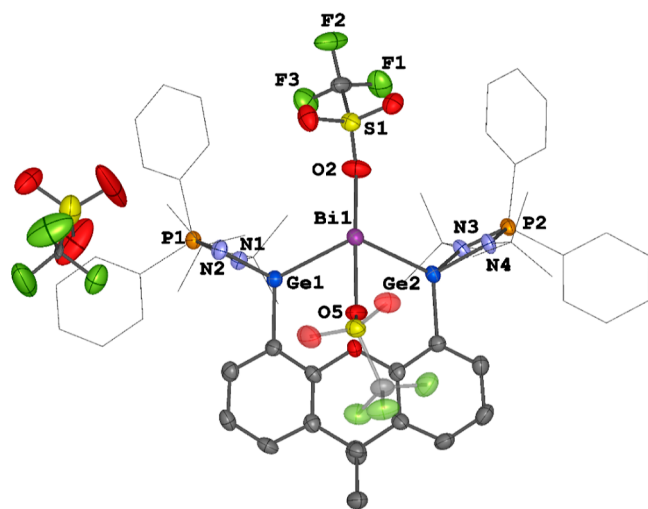

Figure 9. Molecular structure of **7**. Thermal ellipsoids are set at the 50% probability. Hydrogen atoms and solvent molecules are omitted for clarity. Selected bond lengths (Å) and angles (deg): Bi1−Ge1 2.7796(8), Bi1−Ge2 2.7670(8), Bi1−O2 2.410(5), Bi1−O5 2.397(5), Ge1−Bi1−Ge2 107.22(2), O5−Bi1−O2 169.85(18).

monoclinic space group $P12_1/c1$. Similar to compounds **2** and **3**, the central Bi^{III} site also adopts a seesaw geometry with the two OTf units located in the axial positions (O5−Bi1−O2:169.85(18)°). There is a strong interaction between these two OTf units and the Bi^{III} atom [Bi−O lengths: 2.410(5) and 2.397(5) Å]. In contrast, one OTf anion is noncoordinated to

the Bi^III center. The Ge−Bi distances in **7** [2.7796(8) and 2.7670(8) Å] are comparable to those of **2** and **3** [2.7497(6) to 2.8035(5) Å].

Reactivity of Bi^I Complex 4[OTf] toward MeOTf. To investigate the nucleophilic character of the Bi^I complexes, we conducted the reaction of **4[OTf]** with electrophilic MeOTf. As expected, the red color of **4[OTf]** faded upon the addition of MeOTf. Multinuclear NMR analysis confirmed the formation of new species **8** (Scheme 6). After workup,

Scheme 6. Reaction of 4[OTf] with MeOTf
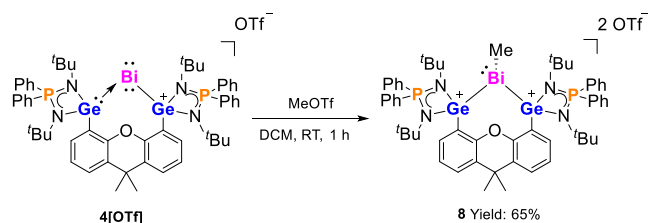
compound **8** was isolated as a pale-yellow powder in 65% yield. Its ^1H NMR spectrum shows two singlets at δ 1.04 and 1.09 ppm, respectively, for the *tert*-butyl groups, implying an asymmetric structure in solution. In addition, the ^1H NMR resonance at δ 2.43 ppm corresponds to the methyl group on the bismuth center, which is downfield shifted compared to that of BiMe$_3$ (δ 1.11 ppm).[73] The $^{31}P\{^1H\}$ NMR spectrum of **8** displays a singlet at δ 53.4 ppm, downfield shifted compared to that of **4[OTf]** (δ 44.5 ppm). The $^{19}F\{^1H\}$ NMR spectrum exhibits a singlet at δ −78.6 ppm, indicating a weak coordinating interaction between the OTf anions and Bi^III atom in solution.

Compound **8** was isolated as pale-yellow crystals and its molecular structure was established by XRD analysis (Figure 10). It crystallizes in the orthorhombic space group $P2_12_12_1$ as an ion triple with a separated dication and two OTf counteranions. The Bi^III center adopts a trigonal pyramidal geometry due to methyl coordination. The Bi−C distance of 2.247(7) Å is shorter than that of $[(TBDSi_2)BiMe][BAr^F]_2$

(2.300 Å).[23] The Ge−Bi distances in **8** of 2.7393(7) and 2.7426(7) Å are longer than those in the two-coordinate Bi^I complex **4** and radical dication **5** (2.6627(4)−2.7147(3) Å), but shorter than those in the four-coordinate **2**, **3**, and **7** (2.7497(6) to 2.8035(5) Å), respectively.

CONCLUSIONS

In summary, two remarkably resonance-stabilized Bi^I complexes, **4[BAr^F]** and **4[OTf]**, supported by an electron-rich chelating bis(iminophosphonamido-germylene) ligand **1**, have been synthesized by reduction of the bis(germylium)Bi^IIII_2 cation precursors **3[BAr^F]** and **3[OTf]** with Cp$_2$Co, respectively. Featuring two lone pairs at the Bi^I atom center, Bi^I cation complex **4** can be considered as an isoelectronic analogue of a Pb^0 complex. Notably, due to the redox noninnocent character of bis(germylene) ligand **1**, the positive charge of Bi^IIII_2 cation in **3** and Bi^I complex **4** migrates to the germanium atoms in **1** which increases the stability of the Bi^III and Bi^I centers substantially. This is also corroborated experimentally by the XPS data. The single-electron oxidation of **4[BAr^F]** with Cp$_2$Fe[BAr^F] furnishes the Bi^II radical complex **5[BAr^F]$_2$** with an unpaired electron located at the Bi^II center and both Ge atoms each featuring one positive charge. Oxidation of **4[OTf]** with 2 M equivs AgOTf and addition of MeOTf affords the Bi^III complexes **7** and **8**, respectively, demonstrating the nucleophilic character of Bi^I cation **4**. We are currently applying these redox-ligand-active Bi^I and Bi^II complexes in photoredox single-electron transfer catalysis in our laboratory. We believe that the stabilization of Bi^I cations and Bi^II radical dication complexes by using redox noninnocent ligands is a promising strategy to gain access to related low-valent p-block metal complexes that are otherwise very difficult to tame.

ASSOCIATED CONTENT

Ⓢ Supporting Information

The Supporting Information is available free of charge at https://pubs.acs.org/doi/10.1021/jacs.3c13016.

Experimental details, materials, and methods, including spectroscopic data and computational data (PDF)

Accession Codes

CCDC 2290234−2290243 contain the supplementary crystallographic data for this paper. These data can be obtained free of charge via www.ccdc.cam.ac.uk/data_request/cif, or by emailing data_request@ccdc.cam.ac.uk, or by contacting The Cambridge Crystallographic Data Centre, 12 Union Road, Cambridge CB2 1EZ, UK; fax: +44 1223 336033.

AUTHOR INFORMATION

Corresponding Authors

Matthias Driess − *Metalorganic and Inorganic Materials, Department of Chemistry, Technische Universität Berlin, 10623 Berlin, Germany;* ⓘ orcid.org/0000-0002-9873-4103; Email: matthias.driess@tu-berlin.de

Gernot Frenking − *State Key Laboratory of Materials-Oriented Chemical Engineering, School of Chemistry and Molecular Engineering, Nanjing Tech University, Nanjing 211816, China; Fachbereich Chemie, Philipps-Universität Marburg, 35032 Marburg, Germany;* ⓘ orcid.org/0000-0003-1689-1197; Email: frenking@chemie.uni-marburg.de
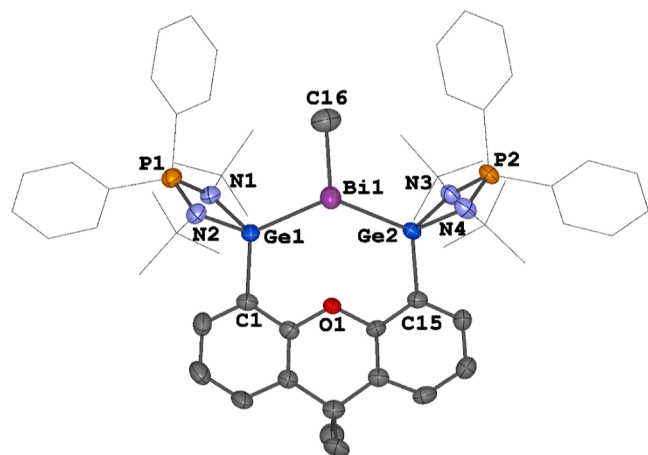
Figure 10. Molecular structure of the dication in **8**. Thermal ellipsoids are set at the 50% probability. Hydrogen atoms, anionic moieties and solvent molecules are omitted for clarity. Selected distances (Å) and angles (deg): Bi1−Ge1 2.7393(7), Bi1−Ge2 2.7426(7), Bi1−C16 2.247(7), Ge1−Bi1−Ge2 108.09(2), C16−Bi1−Ge1 97.6(2), C16−Bi1−Ge2 101.8(2).

Authors

Jian Xu − *Metalorganic and Inorganic Materials, Department of Chemistry, Technische Universität Berlin, 10623 Berlin, Germany*

Sudip Pan − *Institute of Atomic and Molecular Physics, Jilin University, Changchun 130023, China*

Shenglai Yao − *Metalorganic and Inorganic Materials, Department of Chemistry, Technische Universität Berlin, 10623 Berlin, Germany;* ⓘ orcid.org/0000-0002-4005-835X

Christian Lorent − *Physical and Biophysical Chemistry, Department of Chemistry, Technische Universität Berlin, 10623 Berlin, Germany;* ⓘ orcid.org/0000-0001-9057-4523

Christian Teutloff − *Fachbereich Physik, Freie Universität Berlin, 14195 Berlin, Germany;* ⓘ orcid.org/0000-0001-6949-1985

Zhaoyin Zhang − *State Key Laboratory of Materials-Oriented Chemical Engineering, School of Chemistry and Molecular Engineering, Nanjing Tech University, Nanjing 211816, China*

Jun Fan − *Metalorganic and Inorganic Materials, Department of Chemistry, Technische Universität Berlin, 10623 Berlin, Germany*

Andrew Molino − *Department of Chemistry and Physics, La Trobe Institute for Molecular Science, La Trobe University, Melbourne 3086 Victoria, Australia;* ⓘ orcid.org/0000-0002-0954-9054

Konstantin B. Krause − *Institut für Chemie, Humboldt-Universität zu Berlin, 12489 Berlin, Germany;* ⓘ orcid.org/0000-0003-0326-3378

Johannes Schmidt − *Functional Materials, Department of Chemistry, Technische Universität Berlin, 10623 Berlin, Germany*

Robert Bittl − *Fachbereich Physik, Freie Universität Berlin, 14195 Berlin, Germany*

Christian Limberg − *Institut für Chemie, Humboldt-Universität zu Berlin, 12489 Berlin, Germany;* ⓘ orcid.org/0000-0002-0751-1386

Lili Zhao − *State Key Laboratory of Materials-Oriented Chemical Engineering, School of Chemistry and Molecular Engineering, Nanjing Tech University, Nanjing 211816, China;* ⓘ orcid.org/0000-0003-2580-6919

Complete contact information is available at:
https://pubs.acs.org/10.1021/jacs.3c13016

Notes

The authors declare no competing financial interest.

■ REFERENCES

(1) Power, P. P. Main-Group Elements as Transition Metals. *Nature* **2010**, *463*, 171−177.

(2) Yadav, S.; Saha, S.; Sen, S. S. Compounds with Low-Valent p-Block Elements for Small Molecule Activation and Catalysis. *ChemCatChem* **2016**, *8*, 486−501.

(3) Hadlington, T. J.; Driess, M.; Jones, C. Low-Valent Group 14 Element Hydride Chemistry: Towards Catalysis. *Chem. Soc. Rev.* **2018**, *47*, 4176−4197.

(4) Melen, R. L. Frontiers in Molecular p-Block Chemistry: From Structure to Reactivity. *Science* **2019**, *363*, 479−484.

(5) Shan, C.; Yao, S.; Driess, M. Where Silylene−Silicon Centres Matter in the Activation of Small Molecules. *Chem. Soc. Rev.* **2020**, *49*, 6733−6754.

(6) Xiong, Y.; Yao, S.; Inoue, S.; Epping, J. D.; Driess, M. A Cyclic Silylone ("Siladicarbene") with an Electron-Rich Silicon(0) Atom. *Angew. Chem., Int. Ed.* **2013**, *52*, 7147−7150.

(7) Wang, Y.; Karni, M.; Yao, S.; Kaushansky, A.; Apeloig, Y.; Driess, M. Synthesis of an Isolable Bis(Silylene)-Stabilized Silylone and Its Reactivity Toward Small Gaseous Molecules. *J. Am. Chem. Soc.* **2019**, *141*, 12916−12927.

(8) Yao, S.; Kostenko, A.; Xiong, Y.; Ruzicka, A.; Driess, M. Redox Noninnocent Monoatomic Silicon(0) Complex ("Silylone"): Its One-Electron-Reduction Induces an Intramolecular One-Electron-Oxidation of Silicon(0) to Silicon(I). *J. Am. Chem. Soc.* **2020**, *142*, 12608−12612.

(9) Xiong, Y.; Yao, S.; Tan, G.; Inoue, S.; Driess, M. A Cyclic Germadicarbene ("germylone") from Germyliumylidene. *J. Am. Chem. Soc.* **2013**, *135*, 5004−5007.

(10) Zhou, Y. P.; Karni, M.; Yao, S.; Apeloig, Y.; Driess, M. A Bis(Silylenyl)Pyridine Zero-Valent Germanium Complex and Its Remarkable Reactivity. *Angew. Chem., Int. Ed.* **2016**, *55*, 15096−15099.

(11) Wang, Y.; Karni, M.; Yao, S.; Apeloig, Y.; Driess, M. An Isolable Bis(Silylene)-Stabilized Germylone and Its Reactivity. *J. Am. Chem. Soc.* **2019**, *141*, 1655−1664.

(12) Yao, S.; Kostenko, A.; Xiong, Y.; Lorent, C.; Ruzicka, A.; Driess, M. Changing the Reactivity of Zero- and Mono-Valent Germanium with a Redox Non-Innocent Bis(Silylenyl)Carborane Ligand. *Angew. Chem., Int. Ed.* **2021**, *60*, 14864−14868.

(13) Xu, J.; Dai, C.; Yao, S.; Zhu, J.; Driess, M. A Genuine Stannylone with a Monoatomic Two-Coordinate Tin(0) Atom Supported by a Bis(Silylene) Ligand. *Angew. Chem., Int. Ed.* **2022**, *61*, No. e2021140.

(14) Xu, J.; Pan, S.; Yao, S.; Frenking, G.; Driess, M. The Heaviest Bottleable Metallylone: Synthesis of a Monatomic, Zero-Valent Lead Complex ("Plumbylone"). *Angew. Chem., Int. Ed.* **2022**, *61*, No. e202209442.

(15) Chen, M.; Zhang, Z.; Qiao, Z.; Zhao, L.; Mo, Z. An Isolable Bis(Germylene)-Stabilized Plumbylone. *Angew. Chem., Int. Ed.* **2023**, *62*, No. e202215146.

(16) Wang, Y.; Kostenko, A.; Yao, S.; Driess, M. Divalent Silicon-Assisted Activation of Dihydrogen in a Bis(N-Heterocyclic Silylene)-Xanthene Nickel(0) Complex for Efficient Catalytic Hydrogenation of Olefins. *J. Am. Chem. Soc.* **2017**, *139*, 13499−13506.

(17) Takagi, N.; Shimizu, T.; Frenking, G. Divalent E(0) Compounds (E = Si−Sn). *Chem.—Eur. J.* **2009**, *15*, 8593−8604.

(18) Frenking, G.; Tonner, R.; Klein, S.; Takagi, N.; Shimizu, T.; Krapp, A.; Pandey, K. K.; Parameswaran, P. New Bonding Modes of Carbon and Heavier Group 14 Atoms Si−Pb. *Chem. Soc. Rev.* **2014**, *43*, 5106−5139.

(19) Majhi, P. K.; Sasamori, T. Tetrylones An Intriguing Class of Monoatomic Zero-Valent Group 14 Compounds. *Chem.—Eur. J.* **2018**, *24*, 9441−9455.

(20) Yao, S.; Xiong, Y.; Driess, M. A New Area in Main-Group Chemistry: Zerovalent Monoatomic Silicon Compounds and Their Analogues. *Acc. Chem. Res.* **2017**, *50*, 2026−2037.

(21) Yao, S.; Xiong, Y.; Saddington, A.; Driess, M. Entering New Chemical Space with Isolable Complexes of Single, Zero-Valent Silicon and Germanium Atoms. *Chem. Commun.* **2021**, *57*, 10139−10153.

(22) Yao, S.; Saddington, A.; Xiong, Y.; Driess, M. Chelating Bis-Silylenes As Powerful Ligands To Enable Unusual Low-Valent Main-Group Element Functions. *Acc. Chem. Res.* **2023**, *56*, 475−488.

(23) Wang, X.; Lei, B.; Zhang, Z.; Chen, M.; Rong, H.; Song, H.; Zhao, L.; Mo, Z. Isolation and Characterization of Bis(Silylene)-Stabilized Antimony(I) and Bismuth(I) Cations. *Nat. Commun.* **2023**, *14*, 2968.

(24) Yao, S.; Szilvási, T.; Xiong, Y.; Lorent, C.; Ruzicka, A.; Driess, M. Bis(Silylene)-Stabilized Monovalent Nitrogen Complexes. *Angew. Chem., Int. Ed.* **2020**, *59*, 22043−22047.

(25) Wang, Y.; Szilvási, T.; Yao, S.; Driess, M. A Bis(Silylene)-Stabilized Diphosphorus Compound and Its Reactivity as a Monophosphorus Anion Transfer Reagent. *Nat. Chem.* **2020**, *12*, 801−807.

(26) Kumar, V.; Gonnade, R. G.; Yildiz, C. B.; Majumdar, M. Stabilization of the Elusive Antimony(I) Cation and Its Coordination Complexes with Transition Metals. *Angew. Chem., Int. Ed.* **2021**, *60*, 25522−25529.

(27) Deb, R.; Balakrishna, P.; Majumdar, M. Recent Developments in the Chemistry of Pn(I) (Pn = N, P, As, Sb, Bi) Cations. *Chem.—Asian J.* **2022**, *17*, No. e202101133.

(28) Pyykko, P. Relativistic Effects in Structural Chemistry. *Chem. Rev.* **1988**, *88*, 563−594.

(29) Pyykkö, P. Relativistic Effects in Chemistry: More Common than You Thought. *Annu. Rev. Phys. Chem.* **2012**, *63*, 45−64.

(30) Moon, H. W.; Cornella, J. Bismuth Redox Catalysis: An Emerging Main-Group Platform for Organic Synthesis. *ACS Catal.* **2022**, *12*, 1382−1393.

(31) Lichtenberg, C.; Pan, F.; Spaniol, T. P.; Englert, U.; Okuda, J. The Bis(Allyl)Bismuth Cation: A Reagent for Direct Allyl Transfer by Lewis Acid Activation and Controlled Radical Polymerization. *Angew. Chem., Int. Ed.* **2012**, *51*, 13011−13015.

(32) Lichtenberg, C. Well-Defined, Mononuclear Bi^I and Bi^{II} Compounds: Towards Transition-Metal-Like Behavior. *Angew. Chem., Int. Ed.* **2016**, *55*, 484−486.

(33) Wang, F.; Planas, O.; Cornella, J. Bi(I)-Catalyzed Transfer-Hydrogenation with Ammonia-Borane. *J. Am. Chem. Soc.* **2019**, *141*, 4235−4240.

(34) Pang, Y.; Leutzsch, M.; Nöthling, N.; Cornella, J. Catalytic Activation of N$_2$O at a Low-Valent Bismuth Redox Platform. *J. Am. Chem. Soc.* **2020**, *142*, 19473−19479.

(35) Planas, O.; Wang, F.; Leutzsch, M.; Cornella, J. Fluorination of Arylboronic Esters Enabled by Bismuth Redox Catalysis. *Science* **2020**, *367*, 313−317.

(36) Pang, Y.; Leutzsch, M.; Nöthling, N.; Katzenburg, F.; Cornella, J. Catalytic Hydrodefluorination via Oxidative Addition, Ligand Metathesis, and Reductive Elimination at Bi(I)/Bi(III) Centers. *J. Am. Chem. Soc.* **2021**, *143*, 12487−12493.

(37) Mato, M.; Spinnato, D.; Leutzsch, M.; Moon, H. W.; Reijerse, E. J.; Cornella, J. Bismuth Radical Catalysis in the Activation and Coupling of Redox-Active Electrophiles. *Nat. Chem.* **2023**, *15*, 1138−1145.

(38) Zhang, P.; Benner, F.; Chilton, N. F.; Demir, S. Organometallic Lanthanide Bismuth Cluster Single-Molecule Magnets. *Chem* **2022**, *8*, 717−730.

(39) Zhang, P.; Nabi, R.; Staab, J. K.; Chilton, N. F.; Demir, S. Taming Super-Reduced Bi$_2^{3-}$ Radicals with Rare Earth Cations. *J. Am. Chem. Soc.* **2023**, *145*, 9152−9163.

(40) Pugliese, E. R.; Benner, F.; Demir, S. From an Isolable Bismolyl Anion to an Yttrium−Bismolyl Complex with μ-Bridging Bismuth(I) Centers and Polar Covalent Y-Bi Bonds. *Chem.—Eur. J.* **2023**, *29*, No. e202302687.

(41) Pugliese, E. R.; Benner, F.; Demir, S. Isolation of an Organometallic Yttrium Bismuth Cluster and Elucidation of Its Electronic Structure. *Chem. Commun.* **2023**, *59*, 14791−14794.

(42) Siddiqui, M. M.; Sarkar, S. K.; Nazish, M.; Morganti, M.; Köhler, C.; Cai, J.; Zhao, L.; Herbst-Irmer, R.; Stalke, D.; Frenking, G.; Roesky, H. W. Donor-Stabilized Antimony(I) and Bismuth(I)

Ions: Heavier Valence Isoelectronic Analogues of Carbones. *J. Am. Chem. Soc.* **2021**, *143*, 1301−1306.

(43) Deka, R.; Orthaber, A. Carbene Chemistry of Arsenic, Antimony, and Bismuth: Origin, Evolution and Future Prospects. *Dalton Trans.* **2022**, *51*, 8540−8556.

(44) Lichtenberg, C. Molecular Bismuth(III) Monocations: Structure, Bonding, Reactivity, and Catalysis. *Chem. Commun.* **2021**, *57*, 4483−4495.

(45) Lichtenberg, C. Radical Compounds of Antimony and Bismuth. *Encyclopedia of Inorganic and Bioinorganic Chemistry*; Wiley, 2020.

(46) Yang, X.; Reijerse, E. J.; Bhattacharyya, K.; Leutzsch, M.; Kochius, M.; Nöthling, N.; Busch, J.; Schnegg, A.; Auer, A. A.; Cornella, J. Radical Activation of N-H and O-H Bonds at Bismuth(II). *J. Am. Chem. Soc.* **2022**, *144*, 16535−16544.

(47) Turner, Z. R. Bismuth Pyridine Dipyrrolide Complexes: a Transient Bi(II) Species Which Ring Opens Cyclic Ethers. *Inorg. Chem.* **2019**, *58*, 14212−14227.

(48) Ishida, S.; Hirakawa, F.; Furukawa, K.; Yoza, K.; Iwamoto, T. Persistent Antimony- and Bismuth-Centered Radicals in Solution. *Angew. Chem., Int. Ed.* **2014**, *53*, 11172−11176.

(49) Schwamm, R. J.; Harmer, J. R.; Lein, M.; Fitchett, C. M.; Granville, S.; Coles, M. P. Isolation and Characterization of a Bismuth(II) Radical. *Angew. Chem., Int. Ed.* **2015**, *54*, 10630−10633.

(50) Ganesamoorthy, C.; Helling, C.; Wölper, C.; Frank, W.; Bill, E.; Cutsail, G. E.; Schulz, S. From Stable Sb- and Bi-Centered Radicals to a Compound with a Ga = Sb Double Bond. *Nat. Commun.* **2018**, *9*, 87.

(51) Krüger, J.; Wölper, C.; Schulz, S. Stepwise Bi-Bi Bond Formation: From a Bi-Centered Radical to Bi$_4$ Butterfly and Bi$_8$ Cuneane-Type Clusters. *Inorg. Chem.* **2020**, *59*, 11142−11151.

(52) Krüger, J.; Haak, J.; Wölper, C.; Cutsail, G. E.; Haberhauer, G.; Schulz, S. Single-Electron Oxidation of Carbene-Coordinated Pnictinidenes-Entry into Heteroleptic Radical Cations and Metalloid Clusters. *Inorg. Chem.* **2022**, *61*, 5878−5884.

(53) Yang, X.; Reijerse, E. J.; Nöthling, N.; SantaLucia, D. J.; Leutzsch, M.; Schnegg, A.; Cornella, J. Synthesis, Isolation, and Characterization of Two Cationic Organobismuth(II) Pincer Complexes Relevant in Radical Redox Chemistry. *J. Am. Chem. Soc.* **2023**, *145*, 5618−5623.

(54) Nagendran, S.; Sen, S. S.; Roesky, H. W.; Koley, D.; Grubmüller, H.; Pal, A.; Herbst-Irmer, R. RGe(I)Ge(I)R Compound (R = PhC(NtBu)$_2$) with a Ge - Ge Single Bond and a Comparison with the Gauche Conformation of Hydrazine. *Organometallics* **2008**, *27*, 5459−5463.

(55) Takahashi, S.; Sekiguchi, J.; Ishii, A.; Nakata, N. An Iminophosphonamido-Chlorosilylene as a Strong σ-Donating NHSi Ligand: Synthesis and Coordination Chemistry. *Angew. Chem., Int. Ed.* **2021**, *60*, 4055−4059.

(56) Menezes, P. W.; Yao, S.; Beltrán-Suito, R.; Hausmann, J. N.; Menezes, P. V.; Driess, M. Facile Access to an Active γ-NiOOH Electrocatalyst for Durable Water Oxidation Derived From an Intermetallic Nickel Germanide Precursor. *Angew. Chem., Int. Ed.* **2021**, *60*, 4640−4647.

(57) Green, S. P.; Jones, C.; Stasch, A. Stable Magnesium(I) Compounds with Mg-Mg Bonds. *Science* **2007**, *318*, 1754−1757.

(58) Haak, J.; Krüger, J.; Abrosimov, N. V.; Helling, C.; Schulz, S.; Cutsail III, G. E. X-Band Parallel-Mode and Multifrequency Electron Paramagnetic Resonance Spectroscopy of S = 1/2 Bismuth Centers. *Inorg. Chem.* **2022**, *61*, 11173−11181.

(59) Morton, J. R.; Preston, K. F. Atomic Parameters for Paramagnetic Resonance Data. *J. Magn. Reson.* **1978**, *30*, 577−582.

(60) Kramida, A., Ralchenko, Yu., Reader, J. *N. A. T. NIST Atomic Spectra Database (Ver. 5.10)*; National Institute of Standards and Technology: Gaithersburg, MD, 2022. Available: https://physics.nist.gov/asd (accessed November 11, 2023).

(61) Frenking, G.; Hermann, M.; Andrada, D. M.; Holzmann, N. Donor−Acceptor Bonding in Novel Low-Coordinated Compounds of Boron and Group-14 Atoms C−Sn. *Chem. Soc. Rev.* **2016**, *45*, 1129−1144.

(62) Zhao, L.; Hermann, M.; Holzmann, N.; Frenking, G. Dative Bonding in Main Group Compounds. *Coord. Chem. Rev.* **2017**, *344*, 163−204.

(63) Zhao, L.; Pan, S.; Holzmann, N.; Schwerdtfeger, P.; Frenking, G. Chemical Bonding and Bonding Models of Main-Group Compounds. *Chem. Rev.* **2019**, *119*, 8781−8845.

(64) Petz, W.; Frenking, G. Neutral and Charged Group 13−16 Homologs of Carbones EL2 (E = B$^-$−In$^-$; Si−Pb; N$^+$−Bi$^+$, O^{2+}−Te^{2+}). *Adv. Inorg. Chem.* **2022**, *79*, 247−299.

(65) Zhao, L.; Hermann, M.; Schwarz, W. H. E.; Frenking, G. The Lewis Electron-Pair Bonding Model: Modern Energy Decomposition Analysis. *Nat. Rev. Chem* **2019**, *3*, 48−63.

(66) Zhao, L.; Pan, S.; Frenking, G. Energy Decomposition Analysis of the Chemical Bond: Scope and Limitation. *Reference Module in Chemistry, Molecular Sciences and Chemical Engineering*; Elsevier, 2022.

(67) Wu, Z.; Xu, J.; Sokolenko, L.; Yagupolskii, Y. L.; Feng, R.; Liu, Q.; Lu, Y.; Zhao, L.; Fernández, I.; Frenking, G.; Trabelsi, T.; Francisco, J. S.; Zeng, X. Parent Thioketene S-Oxide H$_2$CCSO: Gas-Phase Generation, Structure, and Bonding Analysis. *Chem.—Eur. J.* **2017**, *23*, 16566−16573.

(68) Yang, T.; Andrada, D. M.; Frenking, G. Dative versus Electron-Sharing Bonding in N-Oxides and Phosphane Oxides R$_3$EO and Relative Energies of the R$_2$EOR Isomers (E = N, P; R = H, F, Cl, Me, Ph). A Theoretical Study. *Phys. Chem. Chem. Phys.* **2018**, *20*, 11856−11866.

(69) Jerabek, P.; Schwerdtfeger, P.; Frenking, G. Dative and Electron-Sharing Bonding in Transition Metal Compounds. *J. Comput. Chem.* **2019**, *40*, 247−264.

(70) Bickelhaupt, F. M.; Fonseca Guerra, C.; Mitoraj, M.; Sagan, F.; Michalak, A.; Pan, S.; Frenking, G. Clarifying Notes on the Bonding Analysis Adopted by the Energy Decomposition Analysis. *Phys. Chem. Chem. Phys.* **2022**, *24*, 15726−15735.

(71) Bader, R. F. W. *Atoms in Molecules: A Quantum Theory*; Oxford University Press, 1994; p 438.

(72) Cremer, D.; Kraka, E. Chemical Bonds without Bonding Electron Density — Does the Difference Electron-Density Analysis Suffice for a Description of the Chemical Bond? *Angew. Chem., Int. Ed. Engl.* **1984**, *23*, 627−628.

(73) Ramler, J.; Fantuzzi, F.; Geist, F.; Hanft, A.; Braunschweig, H.; Engels, B.; Lichtenberg, C. The Dimethylbismuth Cation: Entry Into Dative Bi−Bi Bonding and Unconventional Methyl Exchange. *Angew. Chem., Int. Ed.* **2021**, *60*, 24388−24394.